Multiple-Orbit Simulations of Binary Neutron Stars: Equation of State Dependence

In-Saeng Suh

Center for Astrophysics, Department of Physics and Center for Research Computing, University of Notre Dame, Notre Dame, Indiana 46556, USA

E-mail: isuh@nd.edu

Grant J. Mathews and J. Reese Haywood

Center for Astrophysics, Department of Physics, University of Notre Dame, Notre Dame, Indiana 46556, USA

E-mail: gmathews@nd.edu

E-mail: reese.haywood@gmail.com

N. Q. Lan

Hanoi National University of Education, 136 Xuan Thuy, Hanoi, Vietnam and Joint Institute for Nuclear Astrophysics (JINA), University of Notre Dame, Notre Dame, Indiana 46556, USA

E-mail: nquynhlan@hnue.edu.vn

January 2016

Abstract. We study the general relativistic hydrodynamic evolution of neutron stars in binary orbits and analyze the equation of state dependence of the orbits as the stars approach the inner most last stable circular orbit. We show that by employing a conformally flat condition on the metric, one can stably numerically evolve ~ 100 quasi-circular orbits and could straightforwardly extend the calculation to the $\sim 10^4$ orbits needed to follow stars through the LIGO frequency band. We apply this code to orbiting neutron stars in the quasi-circular orbit approximation to both demonstrate the stability of this approach and explore the equation of state dependence of the orbital properties. We employ variety of available realistic neutron star equations of state as well as a $\Gamma = 2$ polytrope. We confirm that both the orbital and emergent gravity wave frequency evolve more slowly for a softer equation of state as the stars approach the innermost stable circular orbit.

PACS numbers: 04.25.D-,04.25.dk, 26.60.Kp, 97.60.Jd, 97.80.-d

Keywords: neutron star binaries, equation of state, numerical relativity, gravity waves

1. Introduction

Current interferemetric gravity wave observatories such as LIGO [1], GEO600 [2], GEO-HF [3, 4], TAMA300 [5] and VIRGO [6] have been taking data for some time [7, 8, 9, 10], while a number of second generation observatories such as Advanced LIGO [11], Advanced VIRGO [12] and KAGRA [13] will soon be online. These observatories seek to detect gravity-wave emission from various sources, e.g. from core collapse supernovae, neutron star orbits, the stochastic cosmic background, etc. [1]. Of the many systems that emit gravitational waves, compact neutron-star and/or black-hole binaries are thought to be the best candidates for detecting gravitational radiation [14]. The number of such systems detectable by Advanced LIGO is estimated [14, 15, 16, 17, 18, 19, 20, 21] to be of order several events per year based upon observed close binary-pulsar systems [22, 23].

To date there have been numerous attempts to calculate theoretical templates for gravity waves from compact binaries based upon numerical and/or analytic approaches (see for example [24, 25, 26, 27, 28, 29, 30, 31, 32, 33]). However, most approaches utilize a combination of Post-Newtonian (PN) techniques supplemented with quasi-circular orbit calculations and then applying full GR for only the last few orbits before disruption. In this paper we report on a general relativistic hydrodynamics approach that can compute many orbits stably and efficiently from the PN regime until the last stable orbits. Here, we establish the numerical stability of this approach based upon many orbit simulations of quasi-circular orbit and show that this approach is straightforwardly scalable to evolve the $\sim 10^4$ orbits within the LIGO frequency range. We also study the equation of state dependence of the orbit periods and associated gravity wave emission.

When binary neutron stars are well separated, the Post-Newtonian (PN) approximation is sufficiently accurate [34]. In the PN scheme, the stars are often treated as point masses, either with or without spin. At third order, for example, it has been estimated [35, 36, 37] that the errors due to assuming the stars are point masses is less than one orbital rotation [35] over the $\sim 16,000$ cycles that pass through the LIGO detector frequency band [14]. Nevertheless, it has been noted in many works [32, 38, 39, 40, 41, 42, 43, 44, 45, 46, 47, 48, 49] that relativistic hydrodynamic effects might be evident even at the separations ($\sim 10-100$ km) relevant to the LIGO window.

Indeed, the templates generated by PN approximations, unless carried out to fifth and sixth order [35, 36], may not be accurate unless the finite size and proper fluid motion of the stars is taken into account. In essence, the signal emitted during the last phases of inspiral depends on the finite size and equation of state (EoS) through the tidal deformation of the neutron stars and the cut-off frequency when tidal disruption occurs.

Numeric and analytic simulations [50, 51, 52, 53, 54, 55, 56, 57, 58] of binary neutron stars have explored the approach to the innermost stable circular orbit (ISCO). While these simulations represent some of the most accurate to date, many simulations have

only followed the evolution for a handful of orbits and are based upon an extrapolation of quasi-circular orbits. With $\sim 16,000$ cycles passing though the LIGO frequency band, it may be questionable whether templates based on only a small number of orbits are sufficiently accurate to describe the full evolution of the system. Moreover, although one can obtain a solution to Einstein equations in the quasi-circular orbit condition, there is no guarantee that the true dynamical evolution of the system actually passes through a given set of quasi-circular solutions.

Accurate templates may eventually require the ability to calculate many orbits, keep track of the radiation back reaction along with relativistic hydrodynamic effects. Ideally, one would like to calculate from the post-Newtonian regime to near the inner most stable circular orbit (ISCO).

Toward that end, we describe in this paper an approach based upon the general relativistic hydrodynamics formalism developed in [39, 41, 59, 60] that can evolve from the post-Newtonian to ISCO regimes in a single calculation. We show that it can quickly and stably compute up to ~ 100 orbits and is straightforwardly scalable to the computation of the continuous evolution through the $\sim 10^4$ orbits in the LIGO window. Here, we report here on the formalism and calculate a large number ~ 100 orbits in the quasi-circular limit to prove its stability. We also analyze the EoS dependence of these quasi-circular orbits and make a preliminary estimate of the emergent gravity wave signal. In a subsequent works we will describe the extraction of the gravity wave signal [61] and evolve the stars through the $\sim 10^4$ orbits of the LIGO window.

This paper is organized as follows. In Section 2 the basic method is summarized and in Section 3 a summary of the relevant equations of state is given. In Section 4 a number of code tests are performed in the quasi-equilibrium circular orbit limit to demonstrate the stability of the technique. The EoS dependence of the gravity wave frequency and the binding energy of the systems in analyzed in Section 5. Conclusions are presented in Section 6.

2. Method

2.1. Field Equations

The field equations and hydrodynamic equations of motion are solved in three spatial dimensions and explained in detail elsewhere [38, 39, 59, 62]. Here, we present a brief summary to introduce the variables relevant to the present discussion. We start with the slicing of spacetime into the usual one-parameter family of hypersurfaces separated by differential displacements in a time-like coordinate as defined in the (3+1) ADM formalism [63, 64].

In Cartesian x, y, z isotropic coordinates, proper distance is expressed as

$$ds^2 = -(\alpha^2 - \beta_i\beta^i)dt^2 + 2\beta_i dx^i dt + \phi^4 \delta_{ij} dx^i dx^j \tag{1}$$

where the lapse function α describes the differential lapse of proper time between two hypersurfaces. The quantity β_i is the shift vector denoting the shift in space-like

coordinates between hypersurfaces. The curvature of the metric of the 3-geometry is described by a position dependent conformal factor ϕ^4 times a flat-space Kronecker delta ($\gamma_{ij} = \phi^4 \delta_{ij}$). This conformally flat condition (together with the maximal slicing gauge, $tr\{K_{ij}\} = 0$) requires [64],

$$2\alpha K_{ij} = D_i \beta_j + D_j \beta_i - \frac{2}{3} \delta_{ij} D_k \beta^k \tag{2}$$

where K_{ij} is the extrinsic curvature tensor and D_i are 3-space covariant derivatives. This conformally flat condition on the metric provides a numerically valid initial solution to the Einstein equations. The vanishing of the Weyl tensor for a stationary system in three spatial dimensions guarantees that a conformally flat solution to the Einstein equations exists.

One consequence of this conformally-flat approximation to the three-metric is that the emission of gravitational radiation is not explicitly evolved. Nevertheless, one can extract the gravitational radiation signal and the back reaction via a multipole expansion [39, 65]. An application to the determination of the gravity wave emission from the quasi-circular orbits computed here is given in a subsequent paper [61]. The advantage of this approximation is that conformal flatness stabilizes and simplifies the solution to the field equations.

As a third gauge condition, one can choose separate coordinate transformations for the shift vector and the hydrodynamic grid velocity to separately minimize the field and matter motion with respect to the coordinates. This set of gauge conditions is key to the present application. It allows one to stably evolve up to hundreds and even thousands of binary orbits without the complexity of other solutions in strong gravity.

Given a distribution of mass and momentum on some manifold, then one first solves the constraint equations of general relativity at each time for a fixed distribution of matter. One then evolves the hydrodynamic equations to the next time step. Thus, at each time slice a solution to the relativistic field equations and information on the hydrodynamic evolution is obtained.

The solution of the field variables ϕ, α, and β^i reduce to simple Poisson-like equations in flat space. The Hamiltonian constraint [64], is used to solve for the conformal factor ϕ [39, 66],

$$\nabla^2 \phi = -2\pi \phi^5 \left[W^2(\rho(1+\epsilon) + P) - P + \frac{1}{16\pi} K_{ij} K^{ij} \right] . \tag{3}$$

In the Newtonian limit, the RHS is dominated [39] by the proper matter density ρ, but in strong fields there are also contributions from the internal energy density ϵ, pressure P, and extrinsic curvature. The source is also significantly enhanced by the generalized curved-space Lorentz factor W,

$$W = \alpha U^t \ = \left[1 + \frac{\sum U_i^2}{\phi^4} \right]^{1/2} \ , \tag{4}$$

where U^t is the time component of the relativistic four velocity and U_i are the covariant spatial components. This factor, W, becomes important near the last stable orbit as the specific kinetic energy of the stars rapidly increases.

In a similar manner [39, 66], the Hamiltonian constraint, together with the maximal slicing condition, provides an equation for the the lapse function,

$$\nabla^2(\alpha\phi) = 2\pi\alpha\phi^5\Big[3W^2[\rho(1+\epsilon)+P] - 2\rho(1+\epsilon) + 3P + \frac{7}{16\pi}K_{ij}K^{ij}\Big] \ . \quad (5)$$

Finally, the momentum constraints yields [64] an elliptic equation for the shift vector [41, 67],

$$\nabla^2\beta^i = \frac{\partial}{\partial x^i}\Big(\frac{1}{3}\nabla\cdot\beta\Big) + 4\pi\rho_3^i \ , \quad (6)$$

where

$$\rho_3^i = 4\alpha\phi^4 S_i + \frac{1}{4\pi}\frac{\partial ln(\alpha/\phi^6)}{\partial x^j}\Big(\frac{\partial\beta^i}{\partial x^j} + \frac{\partial\beta^j}{\partial x^i} - \frac{2}{3}\delta_{ij}\frac{\partial\beta^k}{\partial x^k}\Big) \ . \quad (7)$$

Here the S_i are the spatial components covariant momentum density as defined below.

2.2. Relativistic Hydrodynamics

To solve for the fluid motion of the system in curved spacetime it is convenient to use an Eulerian fluid description [68]. We begin with the perfect fluid stress-energy tensor,

$$T_{\mu\nu} = Pg_{\mu\nu} + (\rho(1+\epsilon)+P)U_\mu U_\nu \ , \quad (8)$$

where U_ν is the relativistic four velocity.

By introducing the usual set of Lorentz contracted state variables it is possible to write the relativistic hydrodynamic equations in a form which is reminiscent of their Newtonian counterparts [68]. The hydrodynamic state variables are: the coordinate baryon mass density,

$$D = W\rho \ \ ; \quad (9)$$

the coordinate internal energy density,

$$E = W\rho\epsilon \ \ ; \quad (10)$$

the spatial three velocity,

$$V^i = \alpha\frac{U_i}{\phi^4 W} - \beta^i \ \ ; \quad (11)$$

and the coordinate momentum density,

$$S_i = (D + E + PW)U_i \ \ . \quad (12)$$

In terms of these state variables, the hydrodynamic equations are as follows: The equation for the conservation of baryon number takes the form,

$$\frac{\partial D}{\partial t} = -6D\frac{\partial\log\phi}{\partial t} - \frac{1}{\phi^6}\frac{\partial}{\partial x^j}(\phi^6 DV^j) \ \ . \quad (13)$$

The equation for internal energy evolution becomes,

$$\begin{aligned}\frac{\partial E}{\partial t} = & -6(E+PW)\frac{\partial\log\phi}{\partial t} - \frac{1}{\phi^6}\frac{\partial}{\partial x^j}(\phi^6 EV^j) \\ & - P\Big[\frac{\partial W}{\partial t} + \frac{1}{\phi^6}\frac{\partial}{\partial x^j}(\phi^6 WV^j)\Big] \ \ . \end{aligned} \quad (14)$$

Momentum conservation takes the form,

$$\begin{aligned}\frac{\partial S_i}{\partial t} = & -6S_i\frac{\partial \log\phi}{\partial t} - \frac{1}{\phi^6}\frac{\partial}{\partial x^j}(\phi^6 S_i V^j) - \alpha\frac{\partial P}{\partial x^i} \\ & + 2\alpha(D+E+PW)(W-\frac{1}{W})\frac{\partial \log\phi}{\partial x^i} + S_j\frac{\partial \beta^j}{\partial x^i} \\ & - W(D+E+PW)\frac{\partial \alpha}{\partial x^i} - \alpha W(D+\Gamma E)\frac{\partial \chi}{\partial x^i} \quad . \end{aligned} \tag{15}$$

where the last term in Eq. (15) is the contribution form the radiation reaction potential χ as defined in [39, 61]. In the quasi-circular orbit approximation we set this term to zero. Including this term allows for a calculation of the realistic complete orbital evolution via gravity-wave emission.

2.3. Angular momentum and orbital frequency

In the quasi-circular approximation (neglecting angular momentum in the radiation field), this system has a Killing vector corresponding to rotation in the orbital plane. Hence, for these calculations the angular momentum is well defined and given by an integral over the space-time components of the stress-energy tensor [69], i.e.,

$$J^{ij} = \int (T^{i0}x^j - T^{j0}x^i)dV. \tag{16}$$

Aligning the z axis with the angular momentum vector then gives,

$$J = \int (xS^y - yS^x)dV. \tag{17}$$

To find the orbital frequency detected by a distant observer corresponding to a fixed angular momentum we employ a slightly modified derivation of the orbital frequency than that of [59]. In asymptotically flat coordinates the angular frequency detected by a distant observer is simply the coordinate angular velocity, i.e., one simply evaluates

$$\omega \equiv \frac{d\phi}{dt} = \frac{U^\phi}{U^0}, \tag{18}$$

In our ADM conformally flat (3+1) curved space, our only task is then to deduce U^ϕ from code coordinates. For this we make a simple polar coordinate transformation keeping our conformally flat coordinates, so

$$U^\phi = \Lambda^\phi_\nu U^\nu = \frac{xU^y - yU^x}{x^2+y^2} \tag{19}$$

Now, the code uses covariant four velocities, $U_i = g_{i\nu}U^\nu = \beta_i U^0 + \phi^4 U^i$. This gives $U^i = U_i\beta_i(W/\alpha)/\phi^4$. Finally, one must density weight and volume average ω over the fluid differential volume elements. This gives,

$$\omega = \frac{\int d^3x\phi^2(D+\Gamma E)[(\alpha/W)(xU_y - yU_x) - (x\beta_y - y\beta_x)]/(x^2+y^2)}{\int d^3x\phi^6(D+\Gamma E)}. \tag{20}$$

This differs slightly from that of [59], but leads to very similar results. A key point in the present application, however, is the implementation of a grid three velocity V^i_G

Table 1. TABLE PRESENTING CENTRAL DENSITY, BARYON MASS, AND GRAVITATIONAL MASS FOR THE FIVE ADOPTED EQUATIONS OF STATE

EoS	ρ_c ($\times 10^{15} g\ cm^{-3}$)	M_B ($M_\odot$)	M_G ($M_\odot$)
$\Gamma = 2$ Polytrope	0.474	1.50	1.40
MW	1.39	1.54	1.40
LS 220	0.698	1.54	~ 1.40
LS 375	0.492	1.54	~ 1.40
GLN	1.56	1.54	1.40

that minimizes the matter motion with respect to U_i and β_i. Hence, the total angular frequency to a distant observer $\omega_{tot} = \omega + \omega_G$, and in the limit of rigid co-rotation, $\omega_{tot} \to \omega_G$, where $\omega_G = xV^y + yV^x$.

For the orbit calculations described here we model corotating stars, i.e. no spin in the corotating frame. This minimizes matter motion on the grid. We at first run the hydrodynamics calculation with viscous damping for sufficiently long time (a few thousand cycles) to relax to a steady state. Then we then run with no damping. In the present application we examine stars at large separations which are in quasi-equilibrium circular orbits and stable hydrodynamic configurations. These orbits span the time from the last several minutes up to orbit inspiral. Our goal is to establish the stability of the multiple orbit hydrodynamic simulation and to examine where the strong field orbit dynamics computed here deviates from the post-Newtonian regime.

3. Equations of state

In the following we utilize several representative equations of state spanning a range from relatively soft to a stiff nuclear matter. The first is a polytropic equation of state as is often employed in the literature, i.e., $p = K\rho^\Gamma$, with $\Gamma = 2$, where in cgs units, $K = 0.0445(c^2/\rho_n)$, and $\rho_n = 2.3 \times 10^{14}$ g cm^{-3}. These parameters, with $\rho_c = 4.74 \times 10^{14}$ g cm^{-3}, produce an isolated star having radius = 17.12 km and baryon mass = 1.5 M$_\odot$. The second is the zero temperature, zero neutrino chemical potential EoS used to model core-collapse supernovae [39, 59, 70]. We label this EoS as MW. The third is the equation of state developed by Lattimer and Swesty [71] with two different choices of compressibility, one having compressibility $K = 220$ MeV, and the other having $K = 375$ MeV. We denote these as LS 220 and LS 375. The fourth EoS has been developed by Glendenning [72]. This EoS has $K = 240$ MeV, which is close the experimental value [73]. We denote this EoS as GLN. Table 1 summarizes the properties of isolated neutron stars generated with each EoS. For each case the baryon mass was chosen to obtain a gravitational mass for each star of $1.4M_\odot$.

In Fig. 1 we plot the equation of state index, Γ versus density, ρ, for the various EoS's considered here. These are compared the simple polytropic $\Gamma = 2$ EoS often

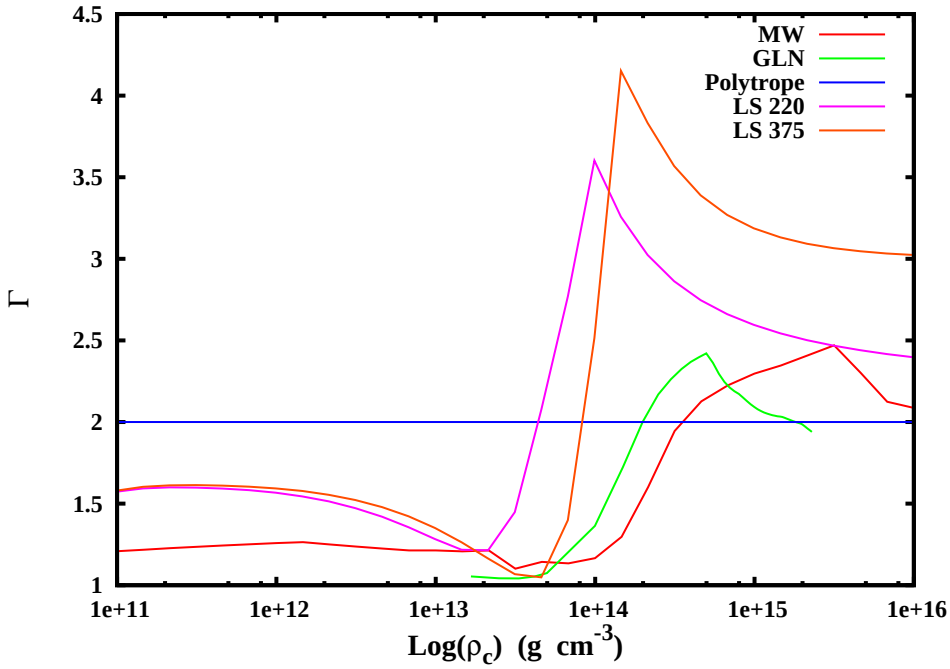

Figure 1. EoS index Γ vs. central density for various equations of state. Large Γ implies a stiff EoS.

employed in the literature.

4. Code validation

4.1. Code Tests

To evolve stars at large separation distance we have decomposed the grid into a high resolution domain with a fine matter grid around the stars and a coarser domain with an extended grid for the fields. Figure 2 shows a schematic of this decomposition.

In the simulations presented here, the number of zones across each star is between 25 and 40 [60]. This keeps the error in the numerics below 0.5%. We utilize an artificial viscosity (AV) shock capturing scheme. An advantage of AV schemes over Riemann solvers is that only about half as many zones are required to accurately resolve the stars when an AV scheme is employed compared to a Riemann solver. Figure 3 shows a plot of orbital velocity vs. time for various Courant parameters. This figure establishes that the routines for the hydrodynamics are stable (e.g. changing the Courant condition has little to effect) as long as $k < 0.5$. Figure 4 illustrates the central density vs. number of zones across the star when calculated with the MW EoS. This figure illustrates that here is only a 1% error in central density with ≈ 15 zones across the star, while increasing the number of zones across the star to > 35 produces less than a 0.1%. In the simulations

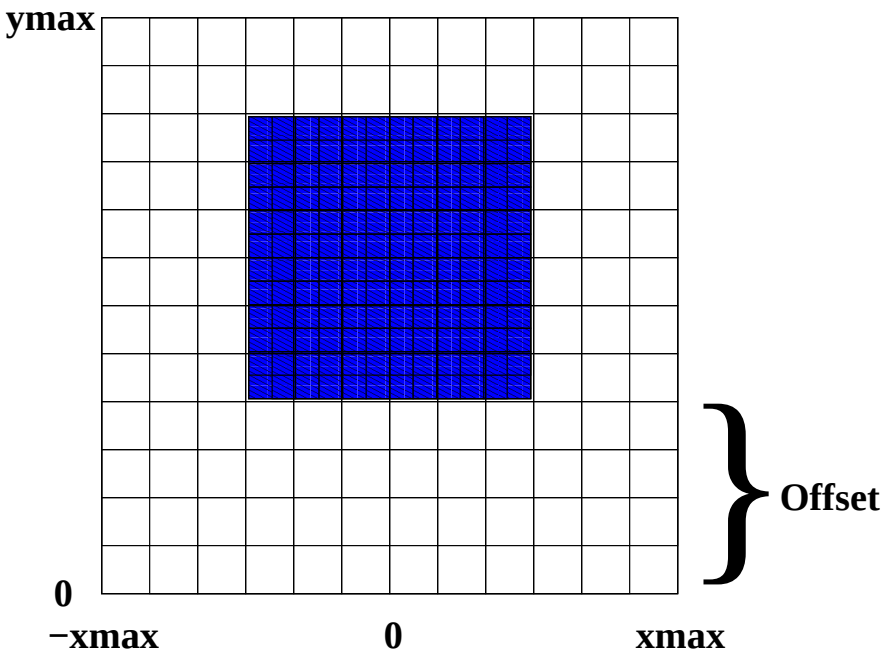

Figure 2. Schematic representation of the field and hydrodynamics grid used in the simulation. The inner blue grid represents the higher resolution matter grid and the outer white grid represents the field grid. The offset will be small for small separations and large for large separations.

below we maintain $k = 0.5$ and ≈ 25 zones across each star as the best choice for both speed and accuracy needed to compute $\sim 16,000$ of orbits [16, 14].

4.2. Orbit stability

As an illustration of the orbit stability a long run was performed in which the angular momentum was fixed at $J = 2.7 \times 10^{11}$ cm^2 and the Courant parameter set to $k = 0.5$. For this orbital calculation we have used the MW EoS and each star was fixed at a baryon mass of $M_B = 1.54$ M$_\odot$ and a gravitational mass in isolation of $M_G = 1.40$ M$_\odot$.

Figure 5 shows the evolution of the orbital angular velocity ω, versus computational cycle for the first 30,000 code cycles corresponding to ≈ 20 orbits. The stars were initially placed on the grid using a solution of the TOV equation in isotropic coordinates for an isolated star. The stars were initially set to be corotating but were allowed to settle into their binary equilibrium. Notice that is takes $\sim 5,000$ cycles, corresponding to ~ 3 orbits, just to approach the quasi-equilibrium binary solution. Indeed, the stars continued to gradually compact and slightly increase in orbital frequency until ~ 10 orbits, afterward, the stars were completely stable. This particular figure extends to ≈ 20 orbits.

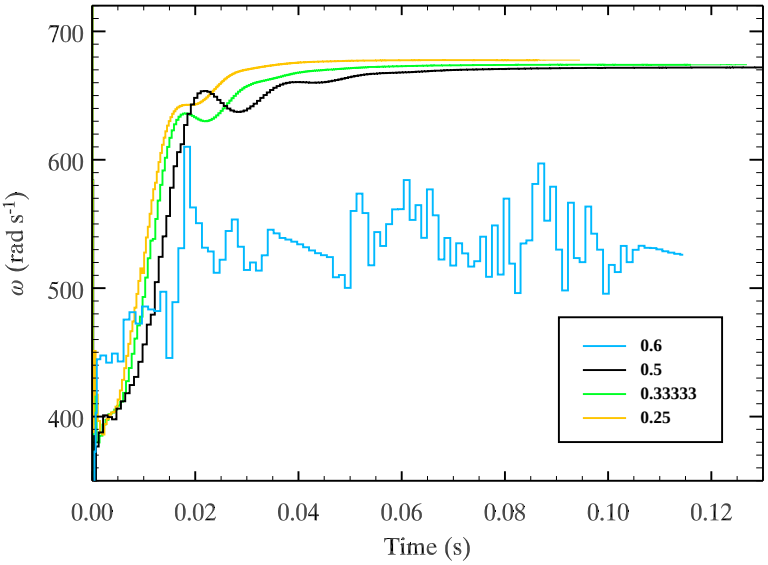

Figure 3. Comparison of the orbital angular velocity ω vs. time for different values of the Courant parameter k. As can be seen, the simulations with $k = 0.25 - 0.5$ result in stable runs that converge to the same value, implying that a smaller k, or equivalently a smaller δt, is not necessary and would only use extra CPU time. For comparison, we plot a simulation with $k = 0.6$ to show that the stability is lost for $k > 0.5$.

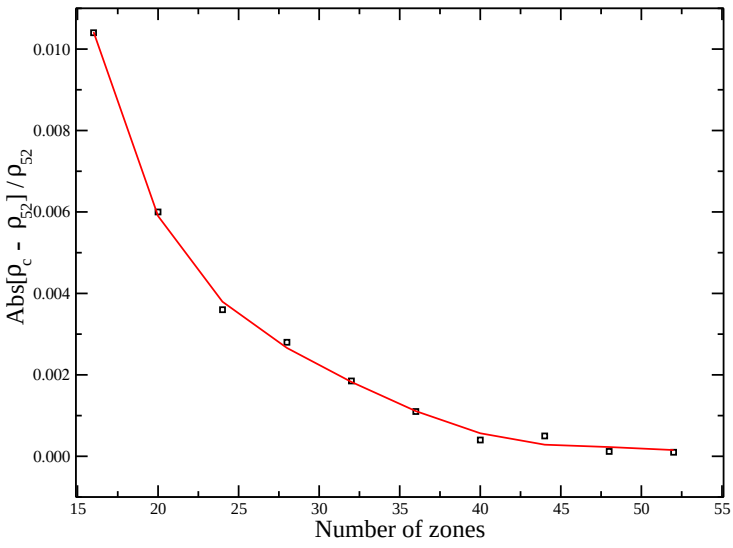

Figure 4. Plot of the error in the central density versus the number of zones across the star. It is clear that there is only a 1% error with ≈ 15 zones across the star. Increasing the number of zones across the star so that there are > 35 zones across the star produces less than a 0.1% error.

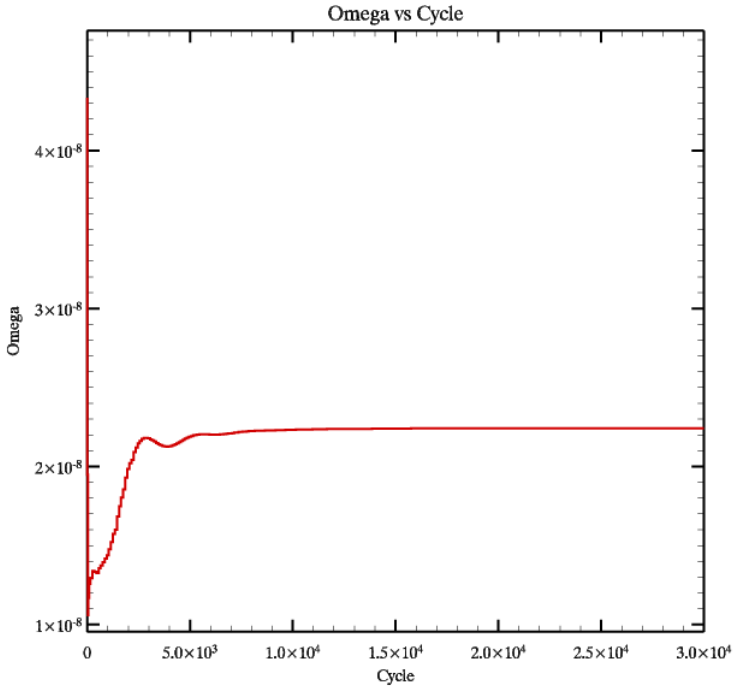

Figure 5. Plot of the orbital angular velocity, ω, versus cycle. When ω stops changing with time the simulation has reached a circular binary orbit solution. This run, which goes over $30,000$ cycles, lasts for ≈ 20 orbits. The geometrized unit of ω in simulation here is used.

Fig. 6 shows the contours of the lapse function α (roughly corresponding to the gravitational potential) and corresponding density profiles at cycle numbers, 0, 5200, and 25800 ($\approx$ 0, 5, and 19 orbits). Figure 7 shows the contours of central density and the orientation of the binary orbit corresponding to these cycle numbers. One can visibly see from these figures the relaxation of the stars after the first few orbits, and the stability of the density profiles after multiple orbits.

We note, however, that this orbit is on the edge of the ISCO. As such it could be unstable to inspiral even after many orbits. Figures 8 and 9 illustrate this point. In these simulations various angular momenta were computed with a slightly higher neutron-star mass ($M_b = 1.61$ M$_\odot$, $M_g = 1.44$ M$_\odot$), but the same MW EoS. In this case the orbits were followed for nearly 100 orbits.

Figure 8 illustrates orbital angular frequency vs. cycle number for three representative angular momenta bracketing the ISCO. The orbital separation for the lowest angular momentum ($J = 2.7 \times 10^{11}$ cm^{-2}) shown on Figure 8 is just inside the ISCO. Hence, even though it requires about 10 orbits before inspiral, the orbit is eventually unstable.

Similarly, Figure 9 shows the central density vs. number of orbits for 11 different angular momenta, five of which have orbits inside the ISCO. Here one can see that only orbits with $J \geq 3.0 \times 10^{11}$ cm^{-2} are stable. Indeed, for these cases, after about the

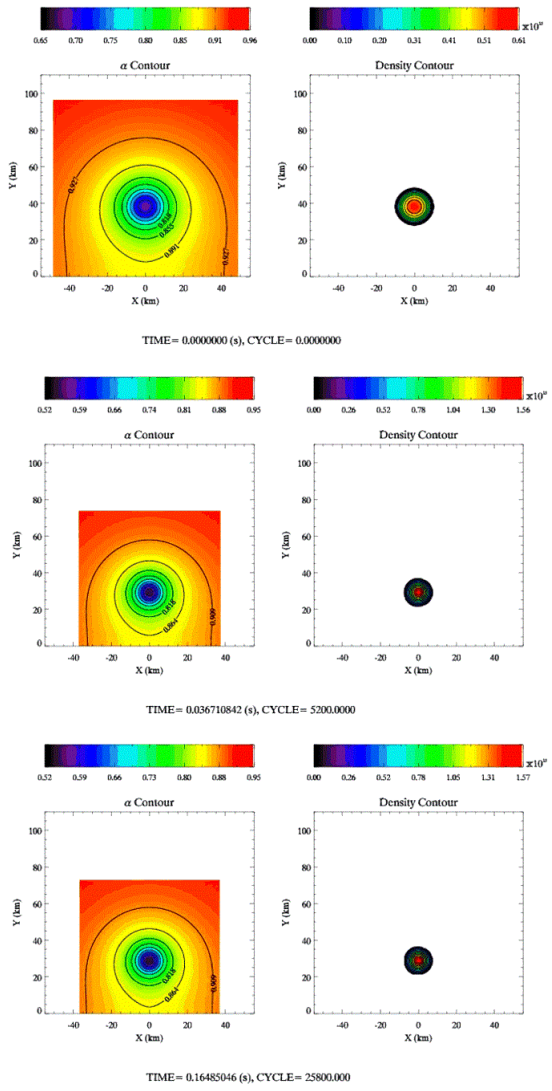

Figure 6. Contours of the lapse function (left) and central density (right) at cycle numbers 0 (top) , 5,200 (middle) , and 25,800 (bottom) corresponding to roughly 0, 5, and 19 orbits.

first 3 orbits the orbits continue with almost no discernible change in orbit frequency or central density. The inference is that one could easily extend this calculation from ~ 100 to $> 10^4$ orbits with no numeric instability. As an illustration of the practicality of that calculation, the run with $J = 3.0 \times 10^{11}$ cm^{-2} required about 2 days (~ 50 hrs) CPU time with an Intel Haswell 2.5 Ghz CPU. Hence 10^4 orbits would require about 7 months of computation with our available platform.

As mentioned previously, the numerical relativistic neutron binary simulations of [50, 51, 52, 53, 54, 55, 56, 57, 58] all start with initial data that are subsequently evolved in a different manner than those with which they were created. One conclusion that may be drawn from the above set of simulations, however, is that the initial data must be evolved for ample time (> 3 orbit) for the stars to reach a true quasi-equilibrium

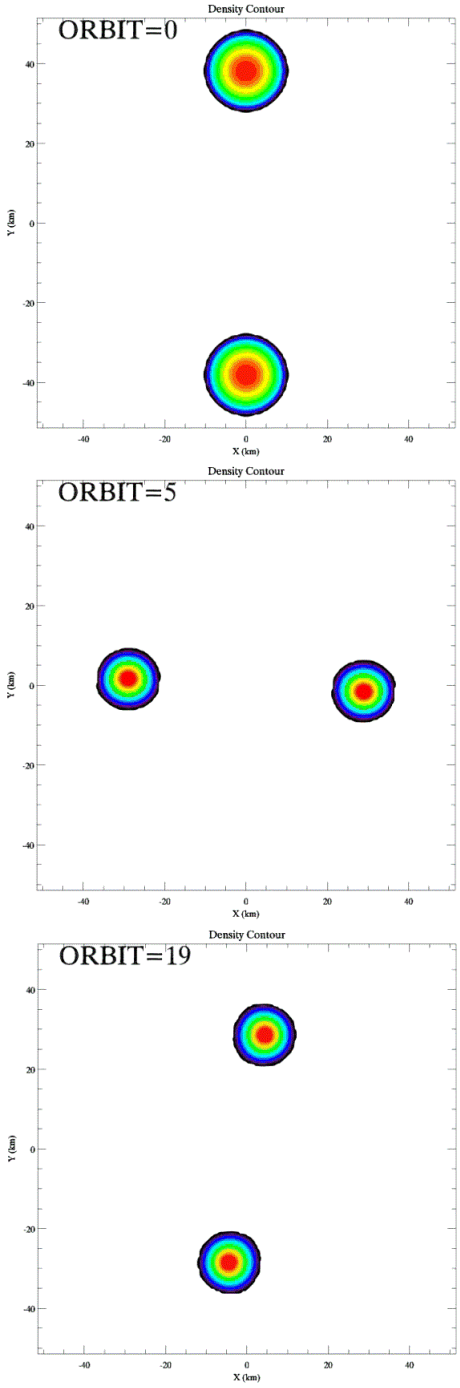

Figure 7. Contours of the central density for the binary system at the approximate number of orbits as labelled.

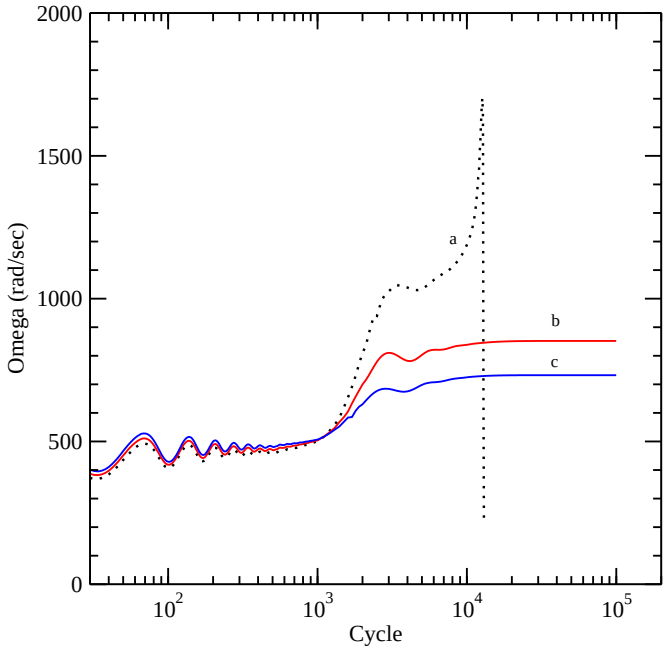

Figure 8. Plot of the orbital angular velocity, ω, versus cycle. When ω stops changing with time the simulation has reached a circular binary orbit solution. The run (a $J = 2.7 \times 10^{11}$ cm^2) goes over ~ 10 obits and then becomes unstable to inspiral and merger after $\sim 10^4$ cycles. The stable two runs (b for $J = 2.8 \times 10^{11}$ cm^{-2} and c for $J = 2.9 \times 10^{11}$ cm^{-2}), were run for $100,000$ cycles, and ≈ 100 orbits.

binary configuration. That has not always been the case.

4.3. Sensitivity of orbital parameters to the equation of state

One hope in the forthcoming detections of gravity waves is that a sensitivity exists to the neutron star equation of state. Hence, having established the stability of the orbits, in Table 2 we summarize the orbit parameters at various fixed angular momenta for the various equations of state considered in this work. In the case of orbits unstable to merger, we list the orbit parameters just before inspiral. These orbits span a range in specific angular momenta J/M_0^2 of ~ 5 to 10. We note that, for comparable angular momenta, our results are consistent with the EoS sensitivity study of [44] based upon a set of equations of state parameterized by a segmented polytropic indices and an overall pressure scale. Their calculations, however, were based upon two independent numerical relativity codes. The similarity of their simulations to our results further confirms the validity of the CFC approach adopted here.

The equations of state listed in Table 2 are in approximate order of increasing stiffness from the top to the bottom. As expected, the central densities are much higher for the relatively soft MW and GLN equations of state. Also, the orbit angular frequencies are considerably different for the extended mass distributions of the stiff equations of state than for the more compact soft equations of state. These extended

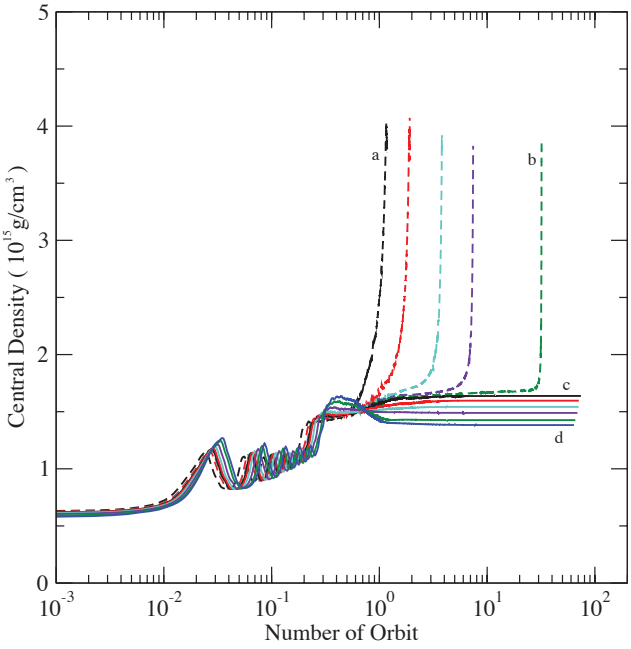

Figure 9. Plot of the central density, ρ_c, versus the number of orbit. The dashed lines from left (a) to right (b) correspond to $J = 2.0, 2.2, 2.4, 2.6, 2.8 \times 10^{11}$ cm^2 and the solid lines from top (c) to bottom (d) are for $J = 3.0, 3.2, 3.4, 3.6, 3.8, 4.0 \times 10^{11}$ cm^2. The case of $J = 2.8 \times 10^{11}$ cm^2 shows stable obits until ~ 30.

mass distributions induce a sensitivity of the emergent gravity wave frequencies and amplitude due to the strong dependence of the gravity wave frequency to the quadrupole moment of the mass distribution.

5. EoS dependence of Gravitational Wave Frequency

The physical processes occurring during the last orbits of a neutron star binary are currently a subject of intense interest. As the stars approach their final orbits it is expected that the coupling of the orbital motion to the hydrodynamic evolution of the stars in the strong relativistic fields could provide insight into various physical properties of the coalescing system [62, 74]. In this regard, careful modeling is needed which includes both the nonlinear general relativistic and hydrodynamic effects as well as a realistic neutron star equation of state.

Fig. 10 shows the EoS sensitivity of the gravity wave frequency in as a function of proper separation d_p between the stars for the various orbits and equations of state summarized in Table 2. These are compared with the circular orbit condition in the (post)$^{5/2}$-Newtonian, hereafter PN, analysis of reference [75]. In that paper a search was made for the inner most stable circular orbit in the absence of radiation reaction terms in the equations of motion. This is analogous to the calculations performed here which

Table 2. Orbital parameters for each EoS

EoS	$J(cm^2)$	$\omega(rad\ s^{-1})$	$d_p(km)$	$d_c(km)$	$M_{ADM}(M_\odot)$	$\rho_c(g\ cm^{-3})$
MW	2.6×10^{11}	780.92	65.22	51.52	1.391	1.67×10^{15}
	2.7×10^{11}	671.85	71.18	57.24	1.393	1.62×10^{15}
	2.8×10^{11}	602.80	76.94	61.86	1.394	1.60×10^{15}
	3.0×10^{11}	482.30	86.91	72.36	1.396	1.55×10^{15}
	3.5×10^{11}	300.46	116.13	100.8	1.399	1.44×10^{15}
	3.8×10^{11}	235.72	136.93	119.74	1.401	1.39×10^{15}
GLN	2.7×10^{11}	666.5	71.62	57.67	1.390	1.73×10^{15}
	2.8×10^{11}	592.34	77.82	62.81	1.391	1.69×10^{15}
	3.0×10^{11}	475.05	88.06	73.53	1.394	1.61×10^{15}
	3.2×10^{11}	391.75	100.34	84.31	1.396	1.56×10^{15}
LS 220	2.7×10^{11}	523.59	90.77	77.34	1.403	7.18×10^{14}
	2.8×10^{11}	472.08	97.53	83.08	1.404	7.14×10^{14}
	3.0×10^{11}	389.96	109.78	94.84	1.405	7.06×10^{14}
	3.2×10^{11}	327.04	122.51	107.10	1.407	6.98×10^{14}
LS 375	2.7×10^{11}	490.09	97.09	83.92	1.404	5.00×10^{14}
	2.8×10^{11}	442.40	103.95	90.04	1.405	4.98×10^{14}
	3.0×10^{11}	366.67	116.65	102.50	1.406	4.95×10^{14}
	3.2×10^{11}	307.80	130.72	115.60	1.407	4.92×10^{14}
Polytrope	1.8×10^{11}	804.70	63.30	51.20	1.395	6.78×10^{14}
	2.1×10^{11}	826.03	67.85	55.18	1.396	7.00×10^{14}
	2.3×10^{11}	762.37	74.64	61.72	1.397	6.55×10^{14}
	2.5×10^{11}	624.33	85.87	72.71	1.399	6.24×10^{14}
	2.6×10^{11}	532.83	94.04	80.45	1.400	6.17×10^{14}
	2.7×10^{11}	477.19	101.34	86.95	1.400	6.05×10^{14}

also analyzes orbit stability in the absence of radiation reaction.

In the $(\text{post})^{5/2}$-Newtonian equations of motion, a circular orbit is derived by setting time derivatives of the separation, angular frequency, and the radial acceleration to zero. This leads to the circular orbit condition [75],

$$\omega_0^2 = mA_0/d_h^3 \quad , \tag{21}$$

where ω_0 is the circular orbit frequency and $m = 2M_G^0$, d_h is the separation in harmonic coordinates, and A_0 is a relative acceleration parameter which for equal mass stars becomes,

$$A_0 = 1 - \frac{3}{2}\frac{m}{d_h}\Big[3 - \frac{77}{8}\frac{m}{d_h} + (\omega_0 d_h)^2\Big] + \frac{7}{4}(\omega_0 d_h)^2 \quad . \tag{22}$$

Equations (21) and (22) can be solved to find the orbit angular frequency as a function of harmonic separation d_h. The gravity wave frequency is then twice the orbit frequency, $f = \omega_0/\pi$.

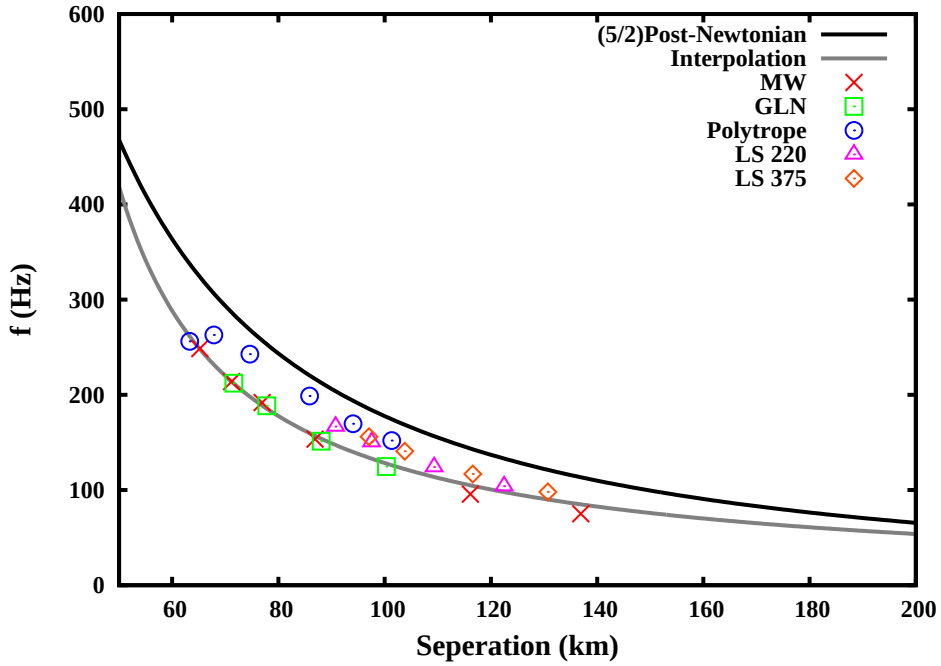

Figure 10. Computed gravitational wave frequency, f, versus proper separation for each EoS as labelled. The black line corresponds to the (post)$^{5/2}$-Newtonian estimate. Frequencies obtained from the stiff and polytropic equations of state do not deviate by more than $\sim 10\%$ from the PN prediction until a frequency greater than ~ 300 Hz. The gray line is an extrapolation of the frequencies obtained using the soft MW and GLN EoSs. These begin to deviate by more than 10% from the PN prediction at a frequency of ~ 100 Hz.

For illustration we show in Fig. 10 the calculated gravitational wave frequency $f = \omega/\pi$ is compared to the PN expectation as a function of proper binary separation distance up to 200 km. Although there is some uncertainty in associating our proper distance with the PN parameter (m/r), it is nevertheless instructive to search for where our strong field calculations deviate from the Post-Newtonian regime. For the polytropic and stiff EoS's there is no significant deviation ($> 10\%$) from the 2.5PN result until frequencies in excess of several hundred Hz. This is consistent with the results of [44] for their multi-segmented polytropic EoSs. We find, however, that for the softer equations of state (MW and GLN) the simulations begin to deviate (by $> 10\%$) from the 2.5PN results for a gravity wave frequency as low as ~ 100 Hz.

Indeed, a striking feature of Figure 10 is that as the stars approach one another, the frequency varies more slowly with diminishing separation distance for the softer equations of state. A gradual change in frequency can mean more orbits in the LIGO window, and hence, a stronger signal to noise. In a subsequent paper [61] we will investigate this point.

Also, for a soft EoS the orbit becomes unstable to inspiral at a larger separation. At least part of this difference can be attributed to the effects of the finite size of the stars rather than point masses. Some of the effect can also be attributed to the slowing of clocks and stretching of distance in the strong field of the neutrons stars [39].

The main parameter characterizing the last stable orbit in the post-Newtonian calculation is the ratio of coordinate separation to total mass (in isolation) d_h/m. The analogous quantity in our non-perturbative simulation is proper separation to gravitational mass, d_P/m. The separation corresponding to the last stable orbit in the post-Newtonian analysis does not occur until the stars have approached 6.03 m. For $M_G^0 = 1.4 M_\odot$ stars, this would correspond to a separation distance of about 25 km. In the results reported here the last stable orbit occurs somewhere just below 7.7 m_G^0 at a proper separation distance of $d_P \approx 30$ km for both the polytropic and the MW stars.

5.1. Binding Energy

Another quantity that may be compared with PN predictions is the binding energy. The binding energy of an isolated star is defined as

$$E_b = M_g - M_0. \tag{23}$$

The total binding energy of the system is defined as

$$E_t = M - 2M_0. \tag{24}$$

In Equations (23) and (24), M_g is the ADM mass of a spherical star in isolation and M_0 is the baryon mass. Also of interest is $M_t = 2M_g$. M is the ADM mass of the binary system and will be different from M_t due to the binding energy between the stars [76]. The (post)^2-Newtonian approximation to the binding energy is given by [76],

$$E_{2PN} = -\eta M_g v^2 \left(1 - \frac{9+\eta}{12} v^2 - \frac{81 - 57\eta + \eta^2}{3} v^4\right) + 2E_b. \tag{25}$$

Here, η is the ratio of the reduced mass to M_t ($\eta = 1/4$ for equal mass binaries) and $v = (M_t \omega)^{1/3}$, where ω is the orbital angular velocity.

The (post)^3-Newtonian approximation has also been derived [35, 36] and is

$$\begin{aligned} E_{3PN} = & -\frac{muv^2}{2}\Big(1 + \left(-\frac{3}{4} - \frac{1}{12}\eta\right) v^2 \\ & + \left\{-\frac{27}{8} + \frac{19}{8}\eta - \frac{1}{24}\eta^2\right) v^4 \\ & + \Big[-\frac{675}{64} + \left(\frac{209323}{4032} - \frac{205}{96}\pi^2 - \frac{110}{9}\lambda\right)\eta \\ & - \frac{155}{96}\eta^2 - \frac{35}{5184}\eta^3\Big] v^6\Big) \quad . \end{aligned} \tag{26}$$

In Figures 11 and 12 we plot the total binding energy per baryon, E_t/M_0 versus v^2. The simulations diverge from the PN results for $v > 0.15$. However, as expected, extending from from 2PN to 3PN diminishes the discrepancy. The simulations which use

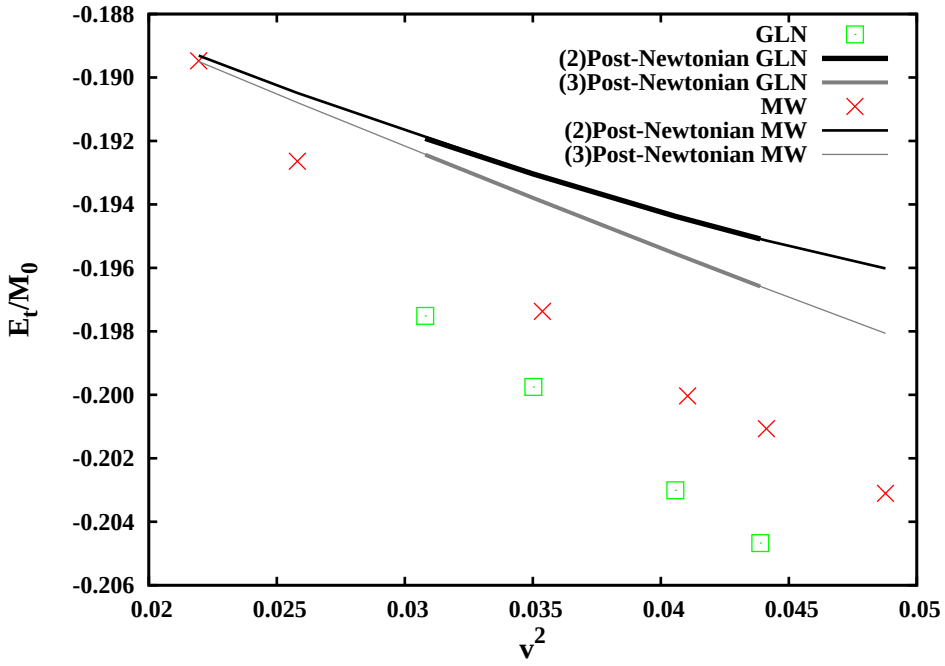

Figure 11. Plot of the total binding energy of the stars, E_t, versus the three-velocity v^2 for the MW and GLN EoS's. This is compared with the 2nd and 3rd order PN prediction. Notice that the 2nd- and 3rdPN approximation to the binding energy is the same for both stars while the simulation begins to deviate for $v > 0.15$.

the MW EoS give the same E_t as the (post)^3-Newtonian solution at angular momentum $J = 3.8 \times 10^{11}$ cm^2. Higher order corrections in the PN expansion should bring agreement between the simulations and the PN expansion at lower J values. This would require (post)^6-Newtonian order, where finite size effects must be taken into account in the expansion [35]. Note also, that even though the gravitational and baryon masses generated with the MW and GLN EoS are the same (see Fig. 10), the resulting binary binding energies are different. Since the gravity wave frequencies are the same, but the binding energies are different, it should be possible to distinguish the "true" EoS from the gravitational wave signal which depends strongly on the mass distribution associated with a given binding energy.

6. Conclusions

We have shown that we can stably evolve the relativistic hydrodynamics of binary neutron star systems over many orbits ($\sim$ 100) and this approach is easily scalable to the $\sim 10^4$ orbits within the LIGO frequency band. We also have shown that such multiple orbit simulations are necessary to precisely determine the location of the ISCO

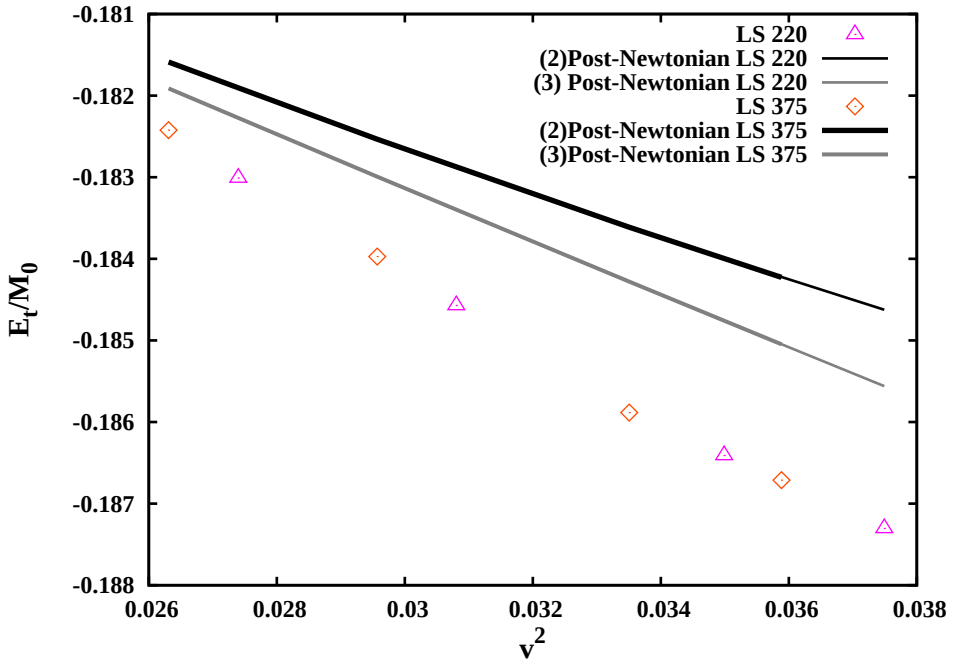

Figure 12. Same as Fig. 11 for the LS 220 and LS 375 EoS's. (Note the change of scale for the horizontal axis).

and the true circular orbit configuration. Moreover, we have examined the sensitivity of the orbit parameters and gravity-wave frequency to the equation of state and confirmed that the orbital properties (e.g. central densities, orbital velocities, binding energies) and location of the ISCO are significantly effected by the stiffness of the EoS. Having established the viability of this approach, in future work a calculation incorporating the gravitational back-reaction will be done to evolve various binary systems through the $\sim 10^4$ orbits of the LIGO window.

Acknowledgements

Work at the University of Notre Dame (G.J.M.) supported by the U.S. Department of Energy under Nuclear Theory Grant DE-FG02-95-ER40934, and by the University of Notre Dame Center for Research Computing. One of the authors (N.Q.L.) was also supported in part by the National Science Foundation through the Joint Institute for Nuclear Astrophysics (JINA) at UND, and in part by the Vietnam Ministry of Education (MOE). N.Q.L. would also like to thank the Yukawa Institute for Theoretical Physics for their hospitality duuring a visit where part of this work was done.

References

[1] LIGO Scientific Collaboration, http://www.ligo.org
[2] GEO Collaboration, Geo600 *http://www.geo600.uni-hannover.de*
[3] Luck H, Affeldt C, Degallaix J, Freise A, Grote H, et al. 2010 *J. Phys. Conf. Ser.* **228** 012012
[4] Affeldt C, Danzmann K, Dooley K, Grote H, Hewitson M, et al. 2014 *Class. Quant. Grav.* **31** 224002
[5] TAMA300 Collaboration, Tama300 *http://tamago.mtk.nao.ac.jp*
[6] VIRGO Collaboration,Virgo *http://wwwcascina.virgo.infn.it*
[7] Abbott B, et al. 2004 *Phys. Rev. D* **69** 082004
[8] Abbott B, et al. 2004 *Phys. Rev. D* **69** 122004
[9] Abbott B and et al. 2006 *Phys. Rev. D* **73** 062001
[10] Abbott B, et al. 2006 *Phys. Rev. D* **73** 102002
[11] Harry G M (LIGO Scientific Collaboration) 2010 *Class. Quant. Grav.* **27** 084006
[12] Acernese F et al. (VIRGO) 2015 *Class. Quant. Grav.* **32** 024001
[13] Somiya K (KAGRA Collaboration) 2012 *Class. Quant. Grav.* **29** 124007
[14] Thorne K S 1996 *Compact Stars in Binaries*, J. van Paradijs, E. P. J. van den Heuvel, and E. Kuulkers, editors, IAU Symp. **165** 153
[15] Harry G M 2010 *Class. Quant. Grav.* **27** 084006
[16] Rasio F A and Shapiro S L1999 *Class. Quant. Grav.* **16** 1
[17] Bailes M 1996 *Compact Stars in Binaries*, J. van Paradijs, E. P. J. van den Heuvel, and E. Kuulkers, editors, IAU Symp. **165** 213
[18] Tutukov A V and Yungelson, L R 1993 *MNRAS* **260** 675
[19] Phinney E S 1991 *Astrophys. J.* **380** L17
[20] Kalogera K et al., 2014 *Astrophys. J. Lett.* **614** L137
[21] Abadie J et al. *Class. Quant. Grav.* **27** 173001
[22] Burgay M et al. 2003 *Nature* **426** 531
[23] Lattimer J M 2012 *Ann. Rev. Nucl Part. Sci* **62** 485
[24] Apostolatos T A 1996 *Phys. Rev. D* **54** 2421
[25] Droz S and Poisson E 1997 *Phys. Rev. D* **56** 4449
[26] Sathyaprakash B S 2000 *Class. Quant. Grav.* **17** L157
[27] Buonanno A, Chen Y, and Vallisneri M 2003 *Phys. Rev. D* **67** 024016
[28] Bose S 2005 *Phys. Rev. D* **71** 082001
[29] Ott C D, Burrows A, Dessart L, and Livne E 2006 *Phys. Rev. Lett.* **96** 201102
[30] Ajith P, Fotopoulos N, Privitera S, Neunzert A, Mazumder N and Weinstein A J 2014, *Phys. Rev. D* **89** 084041
[31] Pannarale F, Berti E, Kyutoku K, Lackey,B D and Shibata M 2015 *Phys. Rev. D* **92**081504
[32] Agathos M, Meidam J, Del Pozzo W, Li T G F, Tompitak M, Veitch J, Vitale S, and Van Den Broeck C 2015 *Phys. Rev. D* **92** 023012
[33] Clark, J A, Bauswein, A, Stergioulas, N and Shoemaker D 2015, eprint arXiv:1509.08522
[34] B. Allen B, Anderson W G, Brady P R, Brown D A, and Creighton J D E 2012 *Phys. Rev. D* **85** 122006
[35] Blanchet L 2002 *Living Rev. Relativity* **5** 3
[36] Blanchet L 2014 *Living Rev. Relativity* **17** 2
[37] Mishra C K, Arun K G and Iyer B R 2015, *Phys. Rev. D* **91** 084040
[38] Wilson J R and Mathews G J, 1995 *Phys. Rev. Lett.* **75** 4161
[39] Wilson J R, Mathews G J, and Marronetti P 1996 *Phys. Rev. D* **54** 1317
[40] Mathews G J, Marronetti P, and Wilson J R 1998 *Phys. Rev. D* **58** 043003
[41] Mathews G J, and Wilson J R 2000 *Phys. Rev. D* **61** 127304
[42] Baiotti L, Damour T, Giacomazzo B, Nagar A and Rezzolla L 2010, *Phys. Rev. Lett.* **105** 261101
[43] Bose, Sukanta; Ghosh, Shaon; Ajith, P. 2010 *Class. Quant. Grav* **27** 114001

[44] Read J S, Baiotti L, Creighton J D E, Friedman J L., Giacomazzo B, Kyutoku K, Markakis C, Rezzolla L, Shibata M and Taniguchi K 2013, *Phys. Rev. D* **88** 044042
[45] Maselli A, Gualtieri L and Ferrari, V 2013 *Phys. Rev. D* **88** 104040
[46] Bauswein A and Stergioulas N 2015 *Phys. Rev. D* **91** 124056
[47] Bauswein A and Stergioulas N and Janka, H-T 2015 *EPLA* in press
[48] Fryer C L, Belczynski K, Ramirez-Ruiz E, Rosswog S, Shen, G and Steiner, A W 2015 *Astrophys. J.* **812** 24
[49] Dietrich T, Moldenhauer N, Johnson-McDaniel N K, Bernuzzi S, Markakis C M, Brügmann B and Tichy W 2015 *Phys. Rev. D* **92** 124007
[50] Duez M D, Marronetti P, Shapiro S L and Baumgarte T W 2003 *Phys. Rev. D* **67** 024004
[51] Marronetti P, Duez M D, Shapiro S L and Baumgarte T W 2003 *Phys. Rev. Lett.* **92** 141101
[52] Miller M, Gressman P, and Suen W-M, 2004 *Phys. Rev. D* **69** 064026
[53] Miller M 2005 *Phys. Rev. D* **71** 104016
[54] Miller M 2007 *Phys. Rev. D* **75** 024001
[55] Uryu K, Limousin F, Friedman J L, Gourgoulhon E and Shibata M 2006 *Phys. Rev. Lett.* **97** 171101
[56] Kiuchi K, Sekiguchi Y, Shibata M and Taniguchi K 2009 *Phys. Rev. D* **80** 064037
[57] Bernuzzi, Sebastiano; Nagar, Alessandro; Dietrich, Tim; Damour, Thibault 2015 *Phys. Rev. Lett.* **114** 161103
[58] De Pietri R, Feo A, Maione F and Löffler F 2015 eprint arXiv:1509.08804
[59] Wilson J R and Mathews G J 2003 *Relativistic Numerical Hydrodynamics*, (Cambridge University Press, Cambridge, United Kingdom)
[60] Haywood, J. R. 2006 PhD Thesis, University of Notre Dame
[61] Lan N Q, Suh, I-S Mathews G J and Reese J H 2016 *Comm.. Phys.* Submitted.
[62] Mathews G J and Wilson J R, 1997 *Astrophys. J.* **482** 929
[63] Arnowitt R, Deser S, and Misner C W 2008 *Gen. Rel. Grav.* **40** 1997
[64] York J W Jr 1979 *Sources of Gravitational Radiation* ed Smarr L L (Cambridge University Press, Cambridge, UK) p. 83,
[65] Thorne K S 1980 *Rev. Mod. Phys.* **52** 299
[66] Evans C R 1984 *A Method for Numerical Relativity: Simulation of Axisymmetric Gravitational Collapse and Gravitational Radiation Generation.*, PhD thesis, University of Texas at Austin
[67] Flanagan E E 1999 *Phys. Rev. Lett.* **82** 1354
[68] Wilson J R 1979 *Sources of Gravitational Radiation* ed Smarr L L (Cambridge University Press, Cambridge, UK) p. 423
[69] Misner C W, Thorne K S, and Wheeler J A 1973, *Gravitation* (Freeman, San Francisco)
[70] Mayle R W, Tavani M and Wilson J R, 1993 *Astrophys. J.* **418** 398
[71] Lattimer J Mand Swesty F D 1991 *Nucl. Phys. A* **535** 331
[72] Glendenning N K 1996 Compact stars, nuclear physics, particle physics, and general relativity, (Springer-Verlag,) New York
[73] Garg U 2004 *Nucl Phys. A* **731** 3
[74] Cutler C, Apostolatos T A, Bildsten L, Finn L S, Flanagan E E, Kennefick D, Markovic D M, Ori A, Poisson E and Sussman G J, 1993 *Phys. Rev. Lett.* **70** 2984
[75] Kidder L E, Will C M and Wiseman A G 1993 *Phys. Rev. D* **47** 4183
[76] Shibata M and Uryu K 2001 *Phys. Rev. D* **64** 104017